Classification
Physics Abstracts
32.80P — 42.50V — 42.60D

A frequency-stabilized LNA laser at 1.083 μm : application to the manipulation of helium 4 atoms

N. Vansteenkiste, C. Gerz, R. Kaiser, L. Hollberg (*), C. Salomon and A. Aspect

Laboratoire de Spectroscopie Hertzienne de l'Ecole Normale Supérieure (**) et Collège de France, 24 rue Lhomond, 75005 Paris, France

(*Received 24 January 1991, accepted in final form 12 September 1991*)

Résumé. — Nous décrivons un laser LNA en anneau, monomode, émettant 60 mW à 1.083 μm. Grâce à une technique d'absorption saturée et une modulation de fréquence à haute fréquence, ce laser est asservi directement sur une raie atomique dans une cellule à décharge d'hélium 4. La largeur de raie résiduelle est de 130 kHz. Nous présentons ensuite deux exemples de manipulation d'atomes d'hélium 4 dans l'état métastable, utilisant ce laser : une augmentation de densité du jet atomique d'un facteur 8, obtenue par une mélasse optique à une dimension, et une déflection sélective du jet d'hélium métastable utilisant un faisceau laser avec des fronts d'onde courbés.

Abstract. — We describe a single mode LNA ring laser, which emits 60 mW at 1.083 μm. Thanks to a high frequency F.M. saturated absorption technique, this laser is directly locked to an atomic line in a ^{4}He discharge cell. The residual frequency jitter is 130 kHz. We then present two examples of laser manipulation of helium 4 atoms in the $2\,^3S_1$ metastable state, using this laser : a density increase of the atomic beam by a factor of 8, with one-dimensional optical molasses, and a selective deflection of the metastable helium beam using a laser beam with curved wavefronts.

1. Introduction.

Since a few years, one knows how to cool and trap neutral particles. Experiments on laser manipulation of atoms such as sodium, cesium, rubidium, lithium, calcium, magnesium, neon and argon, have been performed with various goals : investigation of laser cooling mechanisms, trapping, collision studies at mK temperatures, realization of monoenergetic atomic beams with high brightness [1-8].

In this paper, we report on laser manipulation of metastable helium atoms using the $2\,^3S \leftrightarrow 2\,^3P$ transition at 1.083 μm. Helium has several specific features. First, it is a simple

(*) *Permanent address :* National Institute of Standards and Technology, 325 Broadway, Boulder, CO 80303, U.S.A.

(**) Laboratoire associé au CNRS et à l'Université Pierre et Marie Curie.

atom for which precise QED calculations can be performed and compared with experiments [9]. Second, because of the small mass, the single photon recoil velocity, which is an important parameter in laser cooling, is quite large (9.2 cm.s^{-1}). Third, ^{4}He has no hyperfine structure and the transitions $2\,^3S_1 \leftrightarrow 2\,^3P_{0,1,2}$ offer an interesting choice of level schemes : for instance, $2\,^3S_1 \leftrightarrow 2\,^3P_1$ has been used as a three level Λ system to achieve laser cooling below the single photon recoil energy [10]. Also, the existence of two isotopes ^{3}He and ^{4}He, respectively fermion and boson, is of major interest in the study of quantum collective effects. Finally, metastable helium is used in collision studies [11] and surface scattering experiments [12] : the possibility of tightly focusing a beam of He*, or of achieving unusually large De Broglie wavelengths, opens a new domain for these studies.

The light at 1.083 μm is conveniently produced using the newly developed LNA lasers, which have been recently used in a variety of experiments such as, for instance, optical pumping of liquid helium at low temperature [13], or high precision spectroscopy of the $2\,^3S_1 \leftrightarrow 2\,^3P_{0,1,2}$ transitions [9]. We describe here our realization of a LNA ring laser having a frequency stability and output power appropriate for the manipulation of metastable helium (Sect. 2 and 3). An output power of 60 mW and a laser linewidth of 130 kHz are obtained. Thanks to a high frequency F.M. technique, the frequency stabilization is made using a single servo loop on the saturated absorption peak in a helium discharge cell (Sect. 3). In the second part of this paper, we present two atomic beam manipulation experiments performed with this frequency controlled laser :

— a transverse cooling (velocity compression) experiment, in which the atomic beam intensity on axis is increased by nearly one order of magnitude (Sect. 4) ;

— an atomic beam deflection experiment using the radiation pressure of a travelling laser wave with curved wavefronts (Sect. 5). This state-selective technique allows one to achieve deflection angles large enough to separate the metastable atoms from the ground state atoms. In addition, we have observed a compression of the transverse velocity distribution that is fully understood with a simple calculation presented in section 5.

2. The LNA laser.

The characteristics of a new solid-state laser material called LNA have already been reported, and LNA lasers have been used for producing the 1.083 μm line of helium [9, 13-15]. LNA stands for $La_{1-x}Nd_xMgAl_{11}O_{19}$, where the doping level x in neodymium ions, responsible for the lasing effect, can be as high as 20 %. The same ions are responsible for the well-known 1.06 μm fluorescence line in Nd : YAG, but in LNA, because of the different lattice, the energy levels are slightly shifted and broadened. The corresponding fluorescence spectrum can be found in reference [13]. This spectrum presents a main peak centered at 1.055 μm and a secondary peak, about two times smaller, centered at 1.081 μm. The widths of these peaks are much broader in LNA than in Nd : YAG. In particular the 1.081 μm line has a width (FWHM) of 8 nm, and it is therefore possible to reach $\lambda = 1.083$ μm, which corresponds to the $2\,^3S \leftrightarrow 2\,^3P$ resonance transition in metastable helium 4.

Our LNA laser is shown in figure 1. The crystal is a 5 mm diameter, 10 mm long cylinder, with its axis along the optical axis. This 10 % Nd-doped ($x = 0.1$) LNA was obtained from LETI [16]. Its end faces are AR coated at 1.08 μm. They make an angle of 2° in order to avoid spurious interference effects. The crystal is longitudinally pumped with the 514.5 nm line of an argon-ion laser and it absorbs 70 % of the 3.5 W pump light. The laser cavity has a X shape ring geometry. The X configuration allows us to use small incidence angles ($\theta \approx 7.5°$) on the two spherical mirrors (100 mm radii) in order to keep the output beam astigmatism small. The total length of the cavity is 1.2 m and the waist in the crystal is about 30 μm at

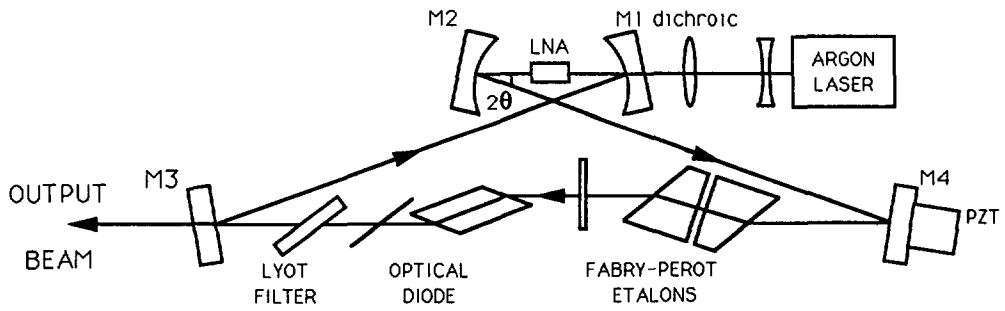

Fig. 1. — The LNA ring laser. The laser cavity is a ring with a X shape (angle of incidence $\theta = 7.5°$), built with two spherical mirrors M_1 and M_2 (radii of curvature $R_{cc} = 100$ mm) and two plane mirrors M_3 and M_4. The LNA crystal (10 mm long, 5 mm diameter, 10 % Nd-doped) is longitudinally pumped with the green line of an argon-ion laser through the dichroic mirror M_1 (94 % transmission at 514.5 nm). The output infrared beam is going out of the cavity through M_3 (4 % transmission at 1.08 μm) ; the other mirrors are high reflectors ($T > 99.9$ %) at this wavelength. The cavity contains (i) an optical diode (10 mm long FR5 Hoya glass in a 3 kg magnetic field plus 0.57 mm thick quartz compensator plate) to enforce unidirectional lasing ; (ii) a Lyot filter made of a 2.3 mm thick birefringent quartz plate ; (iii) a thin Fabry-Perot etalon made of a 0.3 mm thick uncoated glass plate ; (iv) a 3 mm thick air-spaced etalon with 75 % reflection at 1.08 μm (the external faces are at Brewster's angle).

$\lambda = 1.08$ μm. The pump beam is focused on the LNA crystal with a 25 μm waist, through one of the spherical mirrors which has a 94 % transmission at 514.5 nm. Both spherical mirrors M_1 and M_2, and also the plane mirror M_4 are totally reflective at 1.083 μm ($R > 99.9$ %). The plane output coupler M_3 transmits 4 % at that wavelength. In order to avoid spatial hole-burning and to easily obtain single mode operation, we enforce unidirectional operation in the cavity. This is done by an optical diode including a Faraday rotator (FR5 Hoya glass, 10 mm long in a 3 kG magnetic field, yielding a 4° rotation) and an optically active compensator plate (0.57 mm of quartz). Both elements have faces at Brewster's angle and the quartz plate faces are cut at 33° from the optical axis so that the light propagates along the optical axis. The ring cavity containing only this optical diode operates single mode at the maximum gain of LNA, i.e., 1.055 μm.

In order to enforce lasing at 1.08 μm, oscillation on the main peak is suppressed by the insertion of a single birefringent quartz plate with faces parallel to the optical axis (Lyot filter), placed at Brewster's angle (i_B). This plate induces a phase shift [17] :

$$\varphi = \frac{2\pi}{\lambda} e \left\{ n_e \left[1 - \left(\frac{\sin^2 \alpha}{n_e^2} + \frac{\cos^2 \alpha}{n_0^2} \right) \sin^2 i_B \right]^{1/2} - n_0 \left[1 - \frac{\sin^2 i_B}{n_0^2} \right]^{1/2} \right\} \quad (1)$$

where n_0 and n_e are the ordinary and extraordinary indices and α is the angle between the optical axis and the plane of incidence. The thickness of our plate has been chosen in order to avoid laser effect on the main fluorescence peak of LNA at 1.055 μm. We have plotted in figure 2 the calculated efficiency of this birefringent filter in our actual cavity, i.e., the modulus of the largest eigenvalue of the cavity polarization transfer matrix per round trip. It is compared to the transmission spectrum of the same birefringent plate placed between two parallel polarizers. Note that the filter in the cavity is noticeably more selective : this paradoxical result was first pointed out in [18].

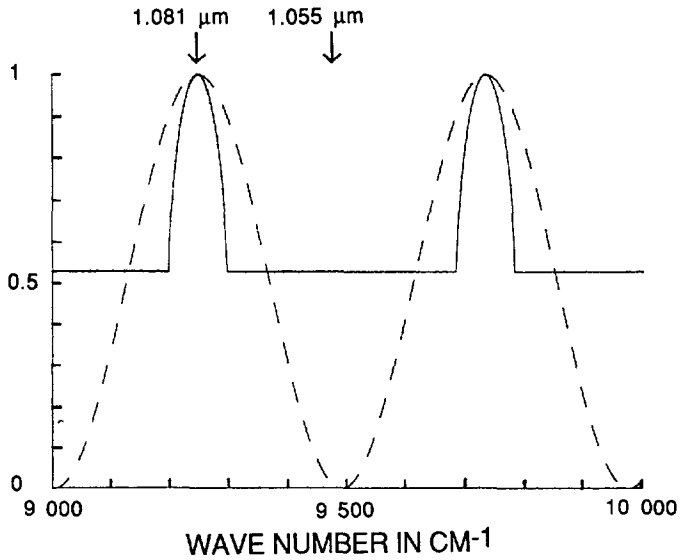

Fig. 2. — Calculated transmission spectrum of the birefringent filter. The filter is a 2.3 mm thick quartz plate, with the optical axis parallel to the faces ; it is placed at Brewster's angle, and can be rotated in this plane, with the optical axis at about 45° from the plane of incidence. The solid line represents the filter's transmission per round trip when it is placed in the cavity of figure 1. The dashed lines is the transmission spectrum of the same plate placed between two parallel polarizers. The thickness of the plate has been chosen so that half the period of the transmission spectrum corresponds to the interval between the 2 fluorescence peaks of LNA (1.055 and 1.081 μm).

Single mode operation at the helium transition (1.083 μm) is obtained by addition of two Fabry-Perot etalons, one 0.3 mm thick uncoated glass plate and a 3 mm air-spaced Fabry-Perot etalon of finesse 10. The thickness of this second Fabry-Perot is controlled with a piezoelectric transducer (PZT) and servoed to the longitudinal mode of the laser cavity. By tuning these three selective elements, lasing has been obtained at any wavelength between 1.078 μm and 1.084 μm. Once having chosen a central frequency in this domain, continuous sweeping over about 1.5 GHz is achieved by changing the cavity length. This is performed using the PZT mount of the M_4 mirror (see Fig. 1).

The output power of the laser, tuned at 1.083 μm, is plotted in figure 3 as a function of the incident power on the LNA crystal at 514 nm. We obtain 60 mW output for 3.5 W of input power, which is more than enough to saturate the $2\,^3S \leftrightarrow 2\,^3P$ transition in ^4He (saturation intensity at resonance $I_S = 0.16\ mW/cm^2$).

We have measured the amplitude noise of the laser by sending part of the beam on a fast photodiode connected to a RF spectrum analyzer. The noise power spectrum is presented in figure 4. Clearly the amplitude noise is significant up to about 500 kHz, beyond which it is close to the shot-noise level. The shape of that spectrum, including the relaxation oscillation peak at 70 kHz, is typical of a solid-state laser [19]. As first pointed out by the authors of [20-22], shot-noise limited detection can then be achieved with frequency modulation techniques at high frequencies (in our case, above 500 kHz). We will show in the next section how we have implemented this technique to make an error signal for stabilizing the laser frequency.

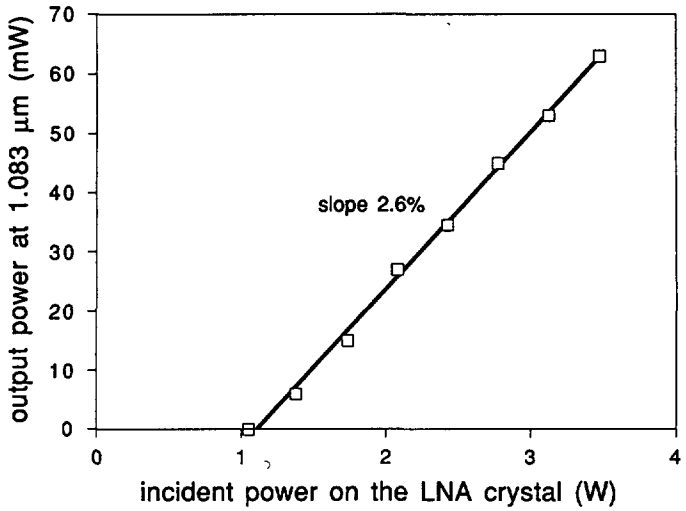

Fig. 3. — Output power of the single mode LNA laser at the helium resonance wavelength (λ = 1.083 μm) as a function of the incident power on the LNA crystal at λ = 514.5 nm. The output coupler M_3 transmits 4 % of the infrared light.

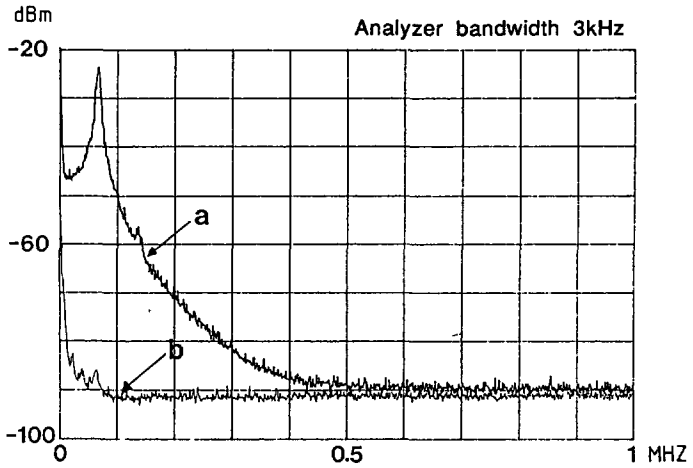

Fig. 4. — Power spectrum of the amplitude noise of the LNA laser. Part of the output beam of the LNA laser is sent on a fast photodiode (quantum efficiency η = 0.12 at 1.08 μm), connected to a radio frequency spectrum analyzer used with a bandwidth of 3 kHz. (a) laser on (1 mW) ; (b) laser off. The noise peak around 70 kHz corresponds to a relaxation oscillation in the crystal. Beyond this frequency, the amplitude noise decreases until 500 kHz where it reaches a constant level, close to the sum of the calculated shot noise and of the measured dark noise of the detection system.

3. Frequency stabilization of the LNA laser.

The frequency noise of the free-running laser is estimated by tuning the laser frequency to the side of a confocal Fabry-Perot cavity (free spectral range 750 MHz, finesse 100) : the total linewidth, measured with a 100 kHz bandwidth detector, is approximately 1 MHz. This value may be too large for some laser cooling experiments on metastable helium 4, since the natural

linewidth of the $2\,^3S_1 \leftrightarrow 2\,^3P_1$ transition is only 1.6 MHz. As a matter of fact, detailed studies of cooling mechanisms require a linewidth significantly smaller than the natural linewidth. Long-term control of the absolute frequency to a fraction of the natural linewidth is also required.

Our first attempts for frequency stabilization of this LNA laser were made using simple standard low modulation frequency techniques (kHz range). The laser was first locked to a confocal Fabry-Perot etalon, which in turn was locked to a saturated absorption line at 1.083 μm in a helium discharge cell. This required two frequency servo loops. The obtained performances (jitter of 750 kHz) were sufficient for our first laser cooling experiments. However we have implemented a more sophisticated stabilization scheme, involving only one servo loop on the saturated absorption signal. This scheme, based on a high frequency modulation technique [20-22], has proved to be considerably more efficient, and we will describe it now.

3.1 ERROR SIGNAL BY F.M. SPECTROSCOPY. — The principle of this technique is to modulate the frequency of the laser beam at a frequency Ω high enough to get rid of the large low frequency technical noise of the laser [20-22]. As shown in figure 4, a frequency above 500 kHz is required for our laser. When the frequency modulated laser beam is passed through a resonant system (atomic line or Fabry-Perot fringe), the frequency modulation at Ω is transformed into an amplitude modulation at Ω, with an amplitude and a phase depending on the detuning from resonance. Demodulation of this signal at Ω provides either a dispersion or an absorption profile around resonance, according to the phase of the demodulation.

We have applied this scheme to the saturated absorption signal in a helium discharge cell. The experimental setup is shown in figure 5. Part of the laser beam is phase modulated at $\Omega = 14.5$ MHz using an electrooptic modulator (EOM) driven by a RF generator. This EOM is a $5 \times 5 \times 12.5$ mm $LiTaO_3$ crystal on which we apply a R.F. transverse electric field parallel to the optical axis. The polarization of the incident laser beam is also parallel to the optical axis : this yields a modulation of the index of refraction (phase modulation) but no amplitude modulation [23]. With a R.F. electric field of about 50 kV/m at $\Omega = 14.5$ MHz (obtained with a resonant circuit), we achieve a phase modulation index $m/\Omega = 0.6$ for the laser field. This beam is then circularly polarized using a polarizing cube and a quarter wave plate and it is sent through the helium discharge cell. Our 120 mm long cell is filled with 0.1 Torr of helium and is excited by a weak RF discharge at 8 MHz to get atoms in the metastable state ($2\,^3S_1$). After passing through the cell, the laser beam is retroreflected and carefully superimposed on the counterpropagating beam in order to get a saturated absorption signal. After the second pass through the quarterwave plate, the polarization is linear again at 90° from the incident one, and it is totally reflected by the polarizing cube, so that the whole retroreflected signal is detected on the fast photodetector. This configuration also avoids unwanted optical feedback into the laser (isolation better than 10^{-2}). The detector is a fast photodiode with a quantum efficiency $\eta = 0.12$ at $\lambda = 1.08$ μm, connected to a current-to-voltage converter with a conversion coefficient of 81 V/mA. The detection system has a bandwidth larger than 20 MHz. Its output signal is heterodyned with the reference in a RF mixer, in order to extract the information at the modulation frequency Ω. We choose the reference phase to obtain a dispersion type signal.

Figure 6 presents the demodulated saturated absorption signal, after a low pass filter with a 7 kHz bandwidth. The width of the line, 25 MHz peak-to-peak, is mostly due to power broadening of the atomic transition (0.1 mW on 1 mm^2). The signal-to-noise ratio is 150 in the 7 kHz bandwidth, that corresponds to 13 000 in a 1 Hz bandwidth. This signal-to-noise ratio is about 200 times larger than in our early version using a 6 kHz modulation. Another factor 6 improvement could be obtained if our detection were shot-noise limited. Actually the

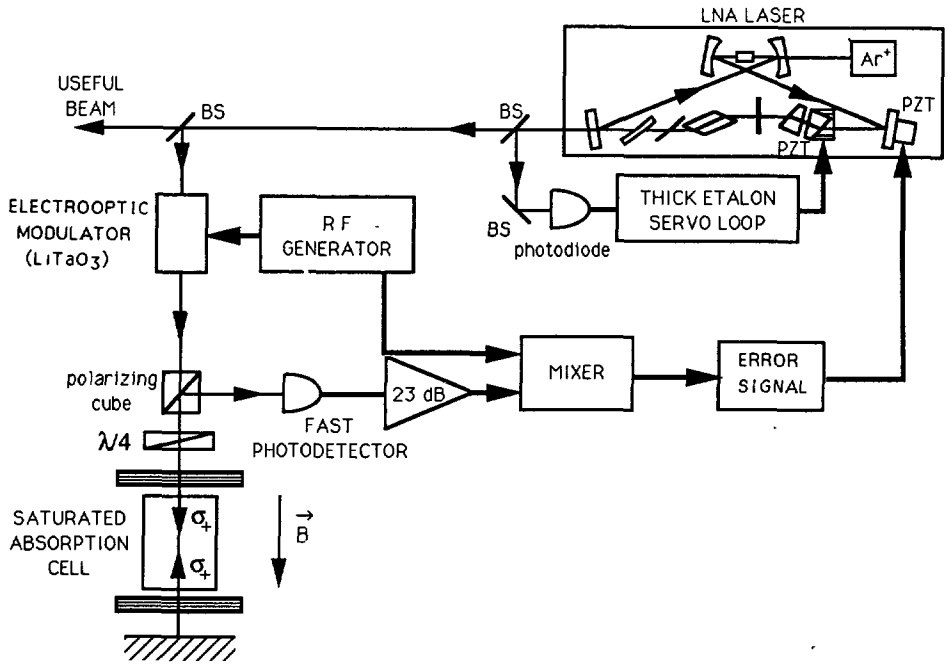

Fig. 5. — Experimental setup for the frequency stabilization of the LNA laser. The laser cavity is directly locked to a saturated absorption line in an helium discharge cell, obtained by using a high frequency phase modulation technique (Ω = 14.5 MHz, modulation index 0.6). The laser frequency is tuned around resonance by Zeeman effect on the atomic resonance line.

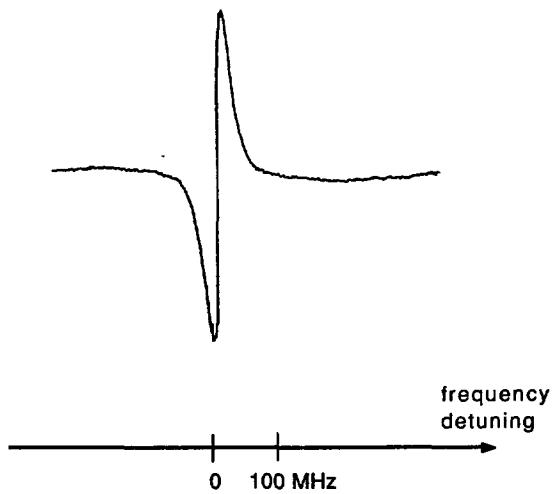

Fig. 6. — Saturated absorption signal ($2\,^3S_1 \leftrightarrow 2\,^3P_2$) as a function of the detuning of the free-running laser with the F.M. spectroscopy scheme of figure 5. The signal-to-noise ratio is 150 in the 7 kHz detection bandwidth. The linewidth is mostly due to power broadening of the atomic transition (the laser intensity in the cell is 0.1 mW on 1 mm^2).

present limitation to the signal-to-noise ratio is mostly due to the noise of the fast amplifier used in the converter.

3.2 FREQUENCY CONTROL AND PERFORMANCES. — The saturated absorption signal produced by the high frequency modulation technique described above is used as an error signal to lock the laser frequency to the atomic transition. The output signal of the mixer is filtered with a 500 kHz bandwidth to get rid of the components at the modulation frequency Ω = 14.5 MHz and its harmonics. This signal is fed into a high voltage amplifier, including an integrator and a filter, having a total transfer function slope of – 9 dB/octave [24]. The output of this amplifier drives the piezo transducer which holds the laser mirror M_4, and controls the frequency of the laser. The gain of the feedback loop is adjusted slightly below the value producing an oscillation at 7.8 kHz.

Figure 7 presents the spectral noise density of the error signal with the locking on (Fig. 7b) and off (Fig. 7a). The dashed line represents the level of noise of the detection system without any light on the photodiode. With this detection noise, the frequency noise of the free-running laser can be measured only below 4 kHz. Taking this frequency noise below 4 kHz, we get an estimation of the linewidth of the free-running laser of about 1 MHz (full width). It is consistent with the observation of the transmission of a confocal Fabry-Perot cavity, tuned at half maximum transmission (FSR 1.5 GHz, finesse 300, detection bandwidth 100 kHz).

For the locked laser (Fig. 7b), the servo loop has a DC gain of about 60 dB and a unity gain at 3 kHz. It allows us to compensate the laser frequency fluctuations in the range where the detection system can measure them. Note that in the range 0 to 1.5 kHz, the error signal goes below the level of the detection noise : it means that the servo loop induces frequency

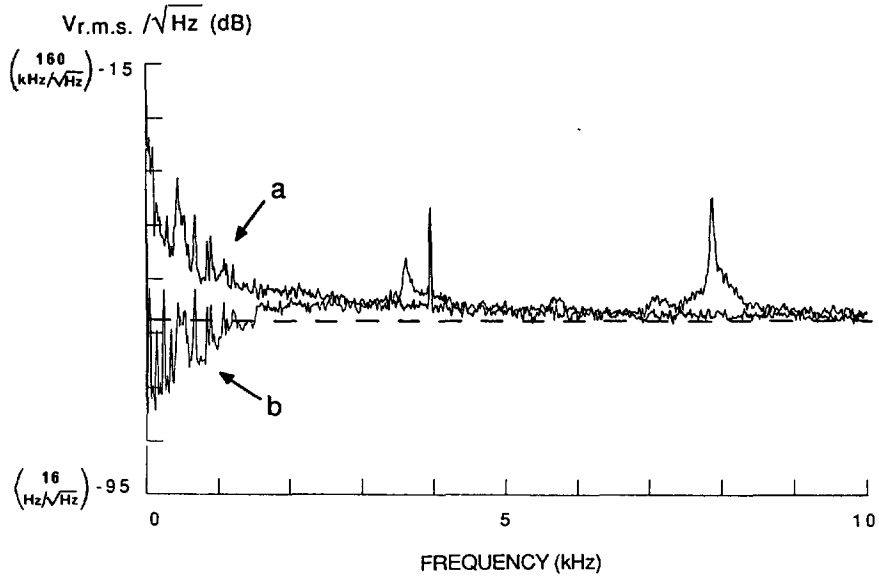

Fig. 7. — Power spectrum of the error signal of the laser frequency stabilization servo loop. The dashed lines correspond to the dark noise level of the detection system (no light on the photodiode). The units are given in dB of $V.Hz^{-1/2}$, with the corresponding value in $Hz.Hz^{-1/2}$ in parenthesis.

(a) free-running laser : most of the measurable frequency noise is below 4 kHz and corresponds to an optical linewidth of about 1 MHz. The sharp peak at 3.95 kHz is due to the modulation applied to the thick etalon inside the cavity.

(b) locked laser : unity gain of the servo loop is reached around 3 kHz. Frequency noise below 3 kHz is well compensated. Note that the servo loop oscillation begins to appear at 7.8 kHz.

fluctuations on the laser correlated with the detection noise. In this range, the true frequency fluctuations of the laser are thus at the level of the detection noise. On the other hand, at frequencies above 3 kHz, the gain of the servo loop is lower than 1, so that it does not deteriorate the spectral density of the free running laser, which remains below the detection noise.

The residual frequency jitter of the locked laser has been evaluated using the same Fabry-Perot cavity as used for the free running laser. We observed frequency fluctuations of about 300 kHz peak-to-peak. This gives an estimation of the linewidth of about 150 kHz. But this is an over-estimation because it also includes the frequency fluctuations of the Fabry-Perot analyzer.

To characterize the spectral properties of the lasers more precisely, we have analyzed the beat note between two LNA lasers of the previously described design. The two lasers are independent except the fact that they are pumped by the same argon-ion laser [25]. Figure 8 shows the power spectrum of the beat signal. Both lasers are locked to the $2\,^3S_1 \leftrightarrow 2\,^3P_2$ transition in separate discharge cells, and one of them is Zeeman detuned (see below) by 2 MHz. The full width at half maximum amounts to 175 kHz. Assuming uncorrelated equal Gaussian distributions for the laser frequency fluctuations, we attribute a linewidth of about 130 kHz to each of the lasers. This value is consistent with the linewidth evaluated above with the confocal Fabry-Perot. We have also determined the Allan variance of the beat note. It decreases from 35 kHz for a measurement time of 100 μs to about 10 kHz between 0.1 s and 100 s. Finally, the reproducibility from day to day is better than 400 kHz.

Once locked to the saturated absorption line, the laser can be tuned by Zeeman shifting the atomic lines in the cell. For this purpose, two coils driven by parallel currents surround the

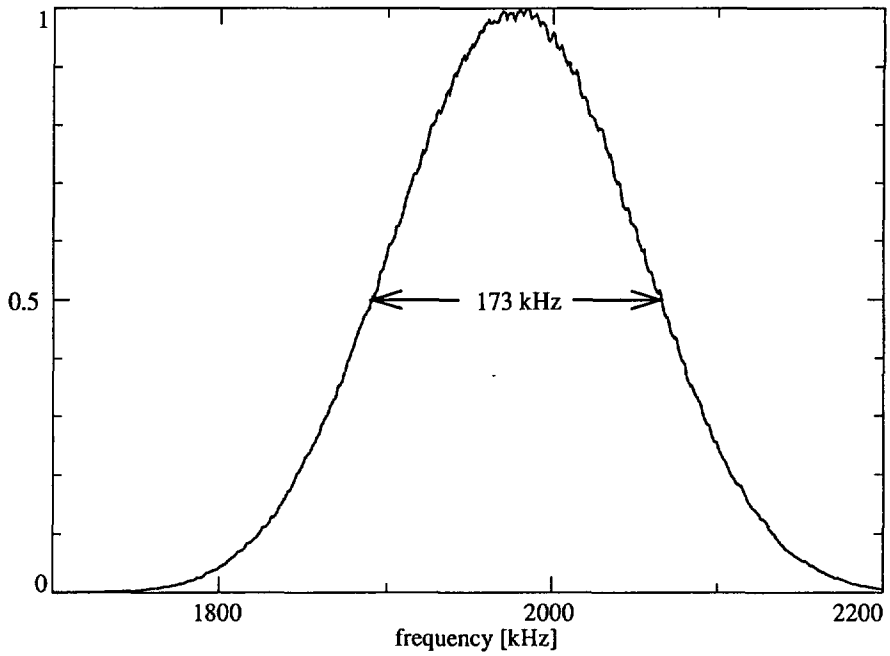

Fig. 8. — Power spectrum of the beat signal between two similar lasers, independently stabilized in frequency. This curve is the average of 100 frequency scans each of which took 2 s. The analyzer resolution of 30 kHz contributes negligibly to the observed width. The curve was smoothed by a 10 Hz video filter.

cell and produce a longitudinal magnetic field homogeneous to about 10 %. The frequency shift depends on the applied magnetic field, on the polarization of the light and on the conditions of the discharge. Consider for example the $2\,^3S_{J=1} \leftrightarrow 2\,^3P_{J=2}$ transition. Because of the σ_+ polarization of the incident light on the cell, optical pumping tends to accumulate the atoms in the $m_J = +1$ sublevel of $2\,^3S_1$. The σ_+ absorption line is thus mostly due to the $m_J = +1 \leftrightarrow m_J = +2$ transition, having a Zeeman shift of 1.4 MHz/Gauss. However, the discharge keeps creating new metastable atoms with equal populations in the three Zeeman sublevels of the $2\,^3S_1$ state, while metastable atoms are quenched to the ground state by various collision mechanisms. These effects compete, and lead to a steady-state distribution of populations in the different sublevels, that depends on the incident laser power and on the discharge conditions. This means that the σ_+ absorption line has in fact three components with different Zeeman shifts and with different weights. For small magnetic fields (less than 5 Gauss), the three lines are not resolved and the position of the maximum, to which the laser is locked, varies linearly with the magnetic field, with a slope that is a weighted average of the three Zeeman shifts. The measured slope is 1.6 MHz/Gauss for the $2\,^3S_1 \leftrightarrow 2\,^3P_2$ line.

3.3 POSSIBLE IMPROVEMENTS. — This LNA laser can be locked to any of the lines of the multiplet $2\,^3S_1 \leftrightarrow 2\,^3P_{0,1,2}$ with a linewidth of 130 kHz and a long term stability better than 0.4 MHz. This is more than sufficient for the cooling experiments described below. For experiments requiring narrower laser linewidth or better long term stability, our system could be easily improved according to the following strategy. The present limiting element is the noise of the fast amplifier responsible for the noise on the error signal. Decreasing the modulation frequency in the megahertz range would allow us to use an amplifier with a lower noise, as well as a photodetector with a higher sensitivity at 1.08 μm. Shot-noise limited detection seems possible along these lines. Another obvious improvement of the signal-to-noise ratio would be to increase the laser power impinging on the detector. One should then expand the laser beam diameter in the cell, in order to keep the intensity at its optimum value, avoiding excessive power broadening of the line and too much bleaching of the absorber. To take full advantage of signal-to-noise ratio improvements, the bandwidth of the frequency correction loop has to be increased. Addition of another fast PZT in the laser cavity, or use of an electro-optic modulator inside (or outside) the cavity are techniques which are now well-mastered [26]. A 1 kHz linewidth could be achieved with a non-limiting feedback electronics and a shot-noise limited detection at 6 mW, assuming a 100 % quantum efficiency for the photodiode (in this case, we would get a spectral noise density of 18 $Hz.Hz^{-1/2}$). To improve long term stability, the discharge cell should be magnetically shielded. This would avoid uncontrolled Zeeman shifts by stray magnetic fields in the laboratory ; in addition, the line in zero magnetic field would be more symmetric and much less sensitive to the conditions of the discharge. Precise detuning from resonance could be achieved by acoustooptic or electrooptic modulators driven by frequency synthesizers. Finally, dc offsets due to linear absorption and parasitic amplitude modulation may be the cause of the long term drifts mentioned above. Modulation transfer techniques would highly reduce this problem.

4. Density increase of a metastable helium beam.

The purpose of the next two sections is to present applications of simple laser cooling techniques to the manipulation of an atomic beam of metastable ^4He, using the LNA laser described previously. In this section, we give a brief description of our metastable helium source and we show how it is possible to increase the atomic density on the beam axis. In section 5, we will discuss the deflection of metastable atoms with a converging laser beam, that allows us to separate the metastable beam from the beam of atoms in the ground state.

4.1 DESCRIPTION OF THE ATOMIC BEAM (Fig. 9). — Our source is a supersonic helium beam excited by a collinear electron gun [27, 28]. The excited atoms decay back to the ground state and to the two metastable states, singlet ($2\,^1S_0$) and triplet ($2\,^3S_1$) (Fig. 10). According to [29], the $2\,^1S_0$ lifetime is 20 ms and the $2\,^3S_1$ lifetime is 7 900 s. The atoms in the singlet

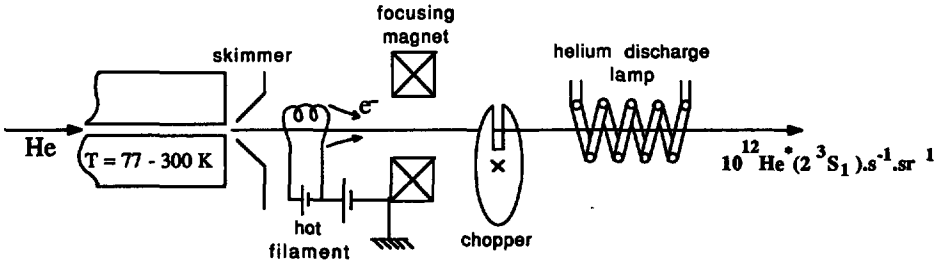

Fig. 9. — Schematic of the $2\,^3S$ metastable helium atomic beam. A supersonic expansion takes place between a container of helium atoms in the ground state (at room temperature or liquid-nitrogen cooled) and a skimmer. The ground state atoms are then bombarded by electrons parallel to the beam, focused by a magnetic field in order to improve the excitation. The atoms excited to the singlet metastable state $2\,^1S_0$ are optically pumped back to the ground state by the light emitted by a helium discharge lamp (see Fig. 10). We measure about 10^{12} atoms per second and per steradian in the $2\,^3S_1$ state. The chopper allows us to determine the velocity distribution by time of flight technique.

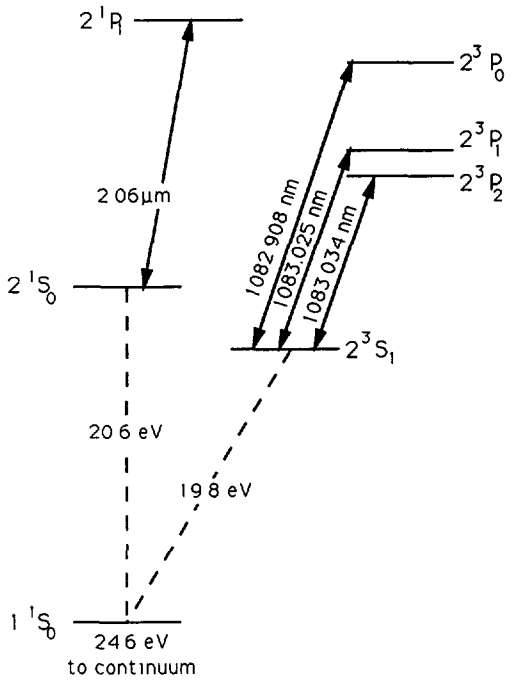

Fig. 10. — First energy levels of helium 4. The atoms in the singlet metastable state $2\,^1S_0$ (lifetime 20 ms) can be excited to $2\,^1P_1$ by radiation at 2.06 μm, and then will most probably decay to the ground state $1\,^1S_0$. Atoms in the triplet metastable state $2\,^3S_1$ (lifetime 7 900 s) can be excited to $2\,^3P_{0,1,2}$ with laser light at 1.083 μm, and will decay back to $2\,^3S_1$ (spin selection rule).

metastable state are optically pumped back to the ground state using the radiation emitted by a helium discharge lamp. Starting with a beam of 10^{18} ground state atoms.s^{-1} sr^{-1} at 300 K, we obtain about 10^{12} metastable triplet atoms.s^{-1}.sr^{-1}

These atoms are detected by taking advantage of their metastability : an electron is emitted when a metastable atom hits the first dynode of an electron multiplier, and the multiplication process produces a measurable pulse at the anode for each detected He* atom. By scanning the electron multiplier perpendicularly to the beam, we can measure the transverse distribution of atoms. The detection is done far enough from the atomic source so that the source can be considered as a point. Knowing the longitudinal velocity of the atoms, we can then deduce the transverse velocity profile.

The longitudinal velocity distribution of the metastable beam depends on the temperature of the initial ground state atoms (300 K or 77 K with liquid-nitrogen cooling) and on the velocity of the electrons. This velocity distribution has been measured for each experiment using a time of flight technique. A typical distribution at 77 K has an average velocity of 1 300 m/s with a dispersion of the order of 10 %.

4.2 ATOMIC DENSITY INCREASE WITH TRANSVERSE LASER COOLING. — Consider an atom with a velocity **v** interacting with a laser travelling wave (wave vector **k**, angular frequency ω_L), quasi resonant with a two-level atomic transition (angular frequency ω_{at}, excited state width Γ). This atom experiences an average radiation pressure force :

$$\mathbf{F} = \hbar\mathbf{k}\,\frac{\Gamma}{2}\,\frac{\omega_1^2/2}{\omega_1^2/2 + \Gamma^2/4 + (\delta - \mathbf{k}\cdot\mathbf{v})^2} \tag{2}$$

where $\delta = \omega_L - \omega_{at}$ is the laser detuning from resonance, and ω_1 is the Rabi frequency characterizing the strength of the interaction between the atom and the laser ($\omega_1^2 = (\Gamma^2/2)(I_L/I_{sat})$, where I_L is the laser intensity, and I_{sat} is the saturation intensity at resonance of the atomic transition). When a metastable helium atom ($2\,^3S_1$) is irradiated by a σ_+ circularly polarized laser beam resonant with the transition $2\,^3S_1 \leftrightarrow 2\,^3P_2$ (Fig. 11), atoms are quickly optically pumped into the cycling transition ($J = 1, m_J = 1$) $\leftrightarrow$ ($J = 2, m_J = 2$). This realizes an effective two level atom. For this transition, $\Gamma/2\pi = 1.6$ MHz and $I_{sat} = 0.16$ mW.cm^{-2}

If the atom is now irradiated by two σ_+ counterpropagating laser waves with the same intensity and frequency (i.e., a standing wave), the total average force is, in the limit of low intensity [30], the sum of the two radiation pressure forces exerted by the two waves :

$$\mathbf{F} = \hbar\mathbf{k}\,\frac{\Gamma}{2}\,\frac{\omega_1^2}{2}\left[\frac{1}{\Gamma^2/4 + (\delta - \mathbf{k}\cdot\mathbf{v})^2} - \frac{1}{\Gamma^2/4 + (\delta + \mathbf{k}\cdot\mathbf{v})^2}\right]. \tag{3}$$

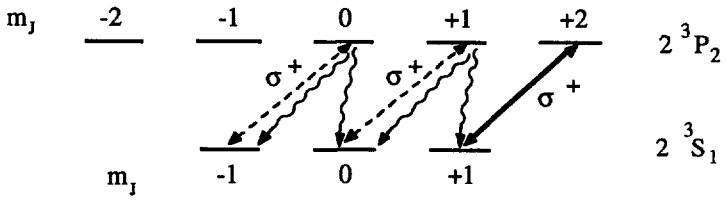

Fig. 11. — $2\,^3S_1$ metastable helium 4 interacting with σ_+ circularly polarized laser light, resonant on the $2\,^3S_1 \leftrightarrow 2\,^3P_2$ transition. By optical pumping, atoms accumulate in the cycling transition $m_J = 1 \leftrightarrow m_J = 2$. This realizes then an effective two level atom.

For a negative detuning ($\omega_L < \omega_{at}$), this force (Fig. 12) is always opposed to the component of the velocity along the wave vector **k** : this velocity component is thus damped. This is the principle of one-dimensional optical molasses [31]. If such a laser standing wave is applied transversely to an atomic beam, the transverse velocity distribution is compressed, and the atomic density on the axis of the atomic beam may be increased. This is interesting for many applications.

The atomic density increase depends in a complicated way on the following factors : laser detuning and intensity, duration of the interaction between the atoms and the laser, geometry of the atomic source, position where the atomic density is measured. A detailed discussion of the influence of these factors is done in [5]. It turns out that the most important factor is the velocity capture range (i.e., the velocity interval over which the damping force is efficient). In order to get the largest density increase, one should have this velocity capture range as large as possible. The choice of parameters allowing one to reach this situation is usually different from the one leading to the narrowest final velocity distribution ($\delta = -\Gamma/2$, $I/I_{sat} \ll 1$).

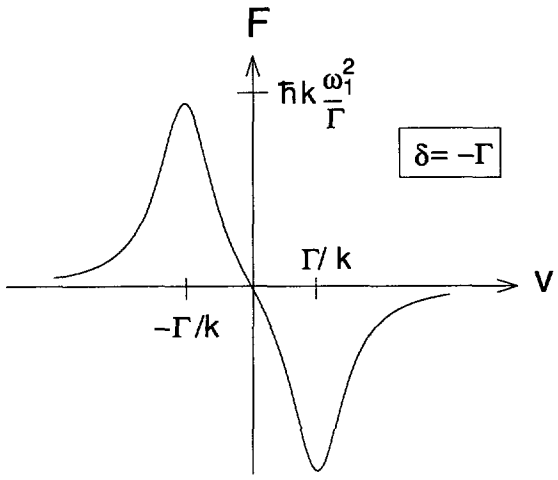

Fig. 12. — Average force exerted on an atom by a low intensity standing wave with a negative detuning ($\delta = -\Gamma$). F and v are the components of the force **F** and of the atomic velocity **v** along the wave vector **k**. At low laser intensity, the two radiation pressure forces from the two counterpropagating waves can be independently added. In the case of this figure (negative detuning), the force damps the atomic velocity.

Figure 13 presents an experimental result where the atomic density on the axis of the beam of $2\,^3S_1$ metastable helium has been increased by a factor of 8 at 2.3 m from the cooling region. In this experiment, the standing wave with an intensity per wave $I = 12\,I_{sat}$ (1.9 mW/cm^2) was applied on a length of 15 mm transversely to the beam (average longitudinal velocity 1 800 m/s) [5]. The detuning yielding the largest density increase was experimentally found equal to $\delta = -1.5\,\Gamma$. Note that this result has been obtained with only a few milliwatts of laser light. With a second standing wave orthogonal to the first one and to the atomic beam, one can reasonably expect to achieve a factor 50 of density increase.

Remark : the above experimental scheme has also been used with a positive detuning, in order to test the purity of the beam of $2\,^3S_1$ atoms. Indeed, for $\delta = \omega_L - \omega_{at}$ positive, the

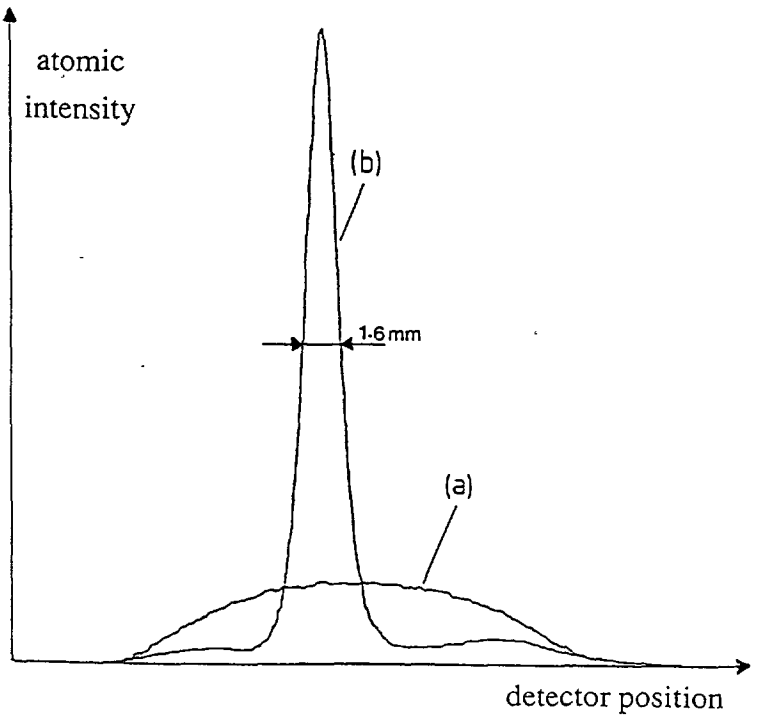

Fig. 13. — Atomic density increase on the axis of an atomic beam, by interaction with a transverse standing wave. The atomic beam profile is analyzed at 2.3 m from the interaction region with an electron multiplier behind a slit of width 1 mm. The transverse dimension of the atomic beam in the interaction region is 1.6 mm. The longitudinal velocity is peaked around 1 800 m/s. (a) laser off ; (b) laser on. The laser beam is a standing wave, 15 mm wide, with an intensity (per travelling wave) equal to $12\, I_{sat}$ (1.9 mW/cm^2). It is detuned 1.5 Γ below resonance.

force exerted by the laser standing wave on the atom (Eq. (3) and Fig. 12) is « anticooling », i.e., has the same sign as the transverse velocity. Atoms interacting with this wave are then efficiently cleared off the center of the beam. By placing the electron multiplier on the axis of the beam, we have been able to adjust the various parameters of the source (electron gun acceleration voltage, quenching discharge lamp...) to completely cancel the signal on the electron multiplier when the expelling laser is applied. We are then sure that the only atomic species producing a signal on the multiplier is helium atoms in the $2\,^3S_1$ state, and that species like $2\,^1S_0$, or Rydberg states have been quenched to a proportion less than 1 %.

5. Atomic beam deflection with a converging laser beam.

As discussed in the section 4, our helium beam contains metastable atoms mixed with about 10^6 times more atoms in the ground state. For some experiments it may be useful to have a pure beam of metastable atoms. We show in this section that a simple radiation pressure deflection technique with a converging laser beam allows one to separate the beam of metastable atoms from the beam of ground state atoms.

5.1 PRINCIPLE. — The radiation pressure force provides an easy way to separate the metastable atoms from the ground state atoms. If a quasi resonant travelling plane wave

illuminates at right angles the atomic beam, the radiation pressure force (Eq. (2)), directed along the laser wave vector **k**, will deflect the metastable atoms from their initial direction [32]. Since this deflection is accompanied by a changing Doppler shift which brings the atoms out of resonance, the deflection process quickly loses its efficiency. At low laser intensity ($\omega_1 \ll \Gamma$), the force will be half of its maximum value as soon as the transverse velocity of the atom has changed by $\Gamma/2k = 0.8$ m/s. With a beam of longitudinal velocity 1 500 m/s, this corresponds to an angle of deviation of only 0.6 mrd. One way to increase the deflection angle would be to use a more intense laser beam, which broadens the resonance line : for example at $\omega_1 = 7\Gamma$ the maximum force is divided by 2 when the transverse velocity of the atom has changed by $\omega_1/(k\sqrt{2}) = 4$ m/s. Another efficient scheme that we present now is to use a converging laser beam. The idea is to keep the atom in resonance with the laser by gradually changing the direction of the wave vector **k** as the atom is deflected, in order to keep $\mathbf{k} \cdot \mathbf{v}$ constant [3, 6]. The radiation pressure force given by equation (2) will then stay constant, close to its maximum value, during the whole interaction time. The angle between the atomic velocity and the wave vector **k** remains constant if we use a converging laser beam with a radius of curvature exactly equal to the curvature of the atomic trajectory (Fig. 14). Such an equilibrium condition is realized only if the radiation pressure force can match the centrifugal inertial force. The detailed calculation presented below yields the range of parameters for which this scheme is efficient. In addition, we will find an interesting cooling effect which gives rise to a compression of the transverse velocity distribution.

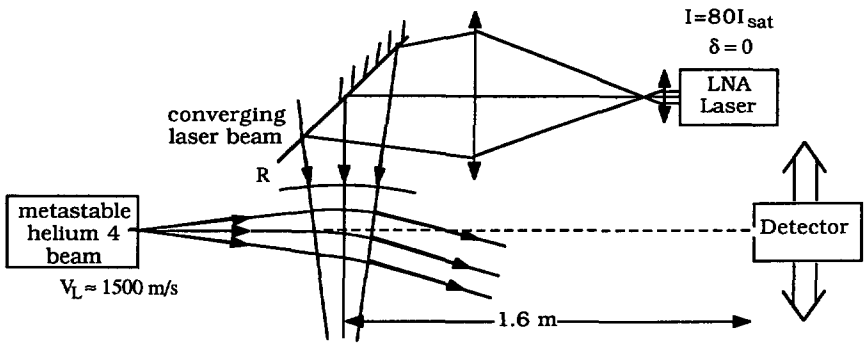

Fig. 14. — Experimental setup for the deflection of the metastable helium beam with a converging laser beam. The radius of curvature of the laser beam ($I = 80\, I_{sat}$, $\delta = 0$) can be modified by changing the length of the telescope. The average longitudinal velocity of the atomic beam is 1 500 m/s, and the deflected atoms are detected with an electron multiplier placed at 1.6 m of the interaction region.

5.2 EQUATION OF MOTION OF AN ATOM IN THE CONVERGING BEAM. — Consider the situation of figure 15. The atomic beam with a direction close to $\mathbf{e}_z$ enters the laser beam at the plane Π_{in}, orthogonal to $\mathbf{e}_z$. The laser beam converges to point O, and is limited by two planes Π_{in} and Π_{out} making an angle α and perpendicular to the plane of the figure. The entrance plane Π_i is chosen quasi perpendicular to the atomic beam. At time $t = 0$, an atom with a velocity **V** in the plane of the figure, enters into the laser beam at point P (OP = R). The initial velocity of the atom in the laboratory frame of reference is $\mathbf{V}(t = 0) = V_y(0)\,\mathbf{e}_y + V_z(0)\,\mathbf{e}_z$ where $(\mathbf{e}_x, \mathbf{e}_y, \mathbf{e}_z)$ are unit vectors of the lab frame $\mathcal{R}$ (see Fig. 15). In order to

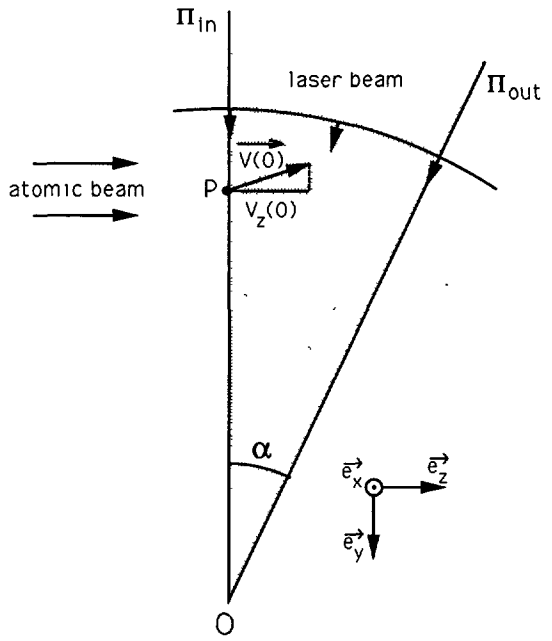

Fig. 15. — Schematic of the interaction region. The laser beam converging at point O is limited by two planes Π_{in} and Π_{out}, making an angle α. An atom enters the laser beam at point P (OP = R) with an initial velocity $\mathbf{V}(0) = V_y(0)\,\mathbf{e}_y + V_z(0)\,\mathbf{e}_z$ in the plane of the figure.

describe the atomic motion in the interaction region, it is convenient to use a frame $\mathcal{R}'(\mathbf{e}_{x'}, \mathbf{e}_{y'}, \mathbf{e}_{z'})$, rotating around O with an angular velocity :

$$\mathbf{\Omega} = -\frac{V_z(0)}{R}\,\mathbf{e}_x . \tag{4}$$

At time $t = 0$, the unit vectors $(\mathbf{e}_{x'}, \mathbf{e}_{y'}, \mathbf{e}_{z'})$ of $\mathcal{R}'$ coincide with $(\mathbf{e}_x, \mathbf{e}_y, \mathbf{e}_z)$ of $\mathcal{R}$. The initial atomic velocity in $\mathcal{R}'$ is thus :

$$\mathbf{V}'(0) = V_y(0)\,\mathbf{e}_y = V_y(0)\,\mathbf{e}_{y'} . \tag{5}$$

We will describe the atomic motion in $\mathcal{R}'$, where the Coriolis acceleration $2\,\mathbf{\Omega} \times \mathbf{V}'(t)$ is negligible compared to the inertial acceleration $\Omega^2 R\mathbf{e}_{y'}$ provided that :

$$|\mathbf{V}'(t)| \ll V_z(0) . \tag{6}$$

In our situation, $V_z(0)$ is about 1 500 m/s whereas $|\mathbf{V}'(0)|$ is smaller than 8 m/s, which corresponds to the divergence of the incident atomic beam. For deflected atoms, the velocity $|\mathbf{V}'(t)|$ in the rotating frame remains of the same order, and condition (6) holds during the whole interaction. In these conditions, the motion of the atom in $\mathcal{R}'$ results from the action of the radiation pressure force $\mathbf{F} = F\mathbf{e}_{y'}$ and of the centrifugal force $-M\Omega^2 R\mathbf{e}_{y'}$. Both forces are central forces. The equation of motion of the atom in $\mathcal{R}'$ writes :

$$M\left[\frac{\mathrm{d}\mathbf{V}'(t)}{\mathrm{d}t}\right]_{\mathcal{R}'} = (F - M\Omega^2 R)\,\mathbf{e}_{y'} . \tag{7}$$

Projecting equation (7) on $\mathbf{e}_{z'}$, we get :

$$M\frac{d\mathbf{V}'(t)\cdot\mathbf{e}_{z'}}{dt}=0 \tag{8}$$

and the component of $\mathbf{V}'(t)$ along $\mathbf{e}_{z'}$ remains zero, according to equation (5). From equation (2), (4) and (7), the component of $\mathbf{V}'(t)$ along $\mathbf{e}_{y'}$ satisfies the equation :

$$M\frac{dV'_{y'}(t)}{dt}=\hbar k\frac{\Gamma}{2}\frac{\omega_1^2/2}{\omega_1^2/2+\Gamma^2/4+(\delta-kV'_{y'}(t))^2}-M\frac{(V_z(0))^2}{R} \tag{9}$$

Note that, in writing (9), we have used :

$$\mathbf{k}\cdot\mathbf{V}(t)=\mathbf{k}\cdot(\mathbf{V}'(t)+R\Omega\mathbf{e}_{z'})=kV'_{y'}(t)\,. \tag{10}$$

We now consider the simple case where the laser intensity is constant along the trajectory of the atom, so that ω_1 is constant [33]. Equation (9) then allows us to make a simple discussion of the motion of the atom in the rotating frame $\mathcal{R}'$. Figure 16 represents the second term of equation (9) as a function of $V'_{y'}$. This term, which is the sum of the radiation pressure and of an inertial centrifugal term, can be interpreted as a total force determining the motion in the rotating frame $\mathcal{R}'$. The two values V'_A and V'_B of the transverse velocity for which this term is zero are steady-state solutions of the equation of evolution of $V'_{y'}$ (Eq. (9)) : V'_A corresponds to an unstable equilibrium whereas V'_B corresponds to a stable equilibrium in the velocity space. An atom with an initial transverse velocity :

$$V'_{y'}>V'_A$$

will have its velocity « attracted » towards V'_B. This condition defines a capture range for the deflection that depends on the laser detuning : for a distribution of $V'_{y'}$ (i.e., transverse velocities) centered around zero, the optimum detuning is around zero. Around V'_B, the slope of the total force is negative, and the evolution of the velocity is damped, until a steady-state is reached. The atom then gets its velocity locked around V'_B [34]. At the end of the interaction region, the trajectory of the atom makes an angle θ_{out} with $\mathbf{e}_z$ (in the lab frame) :

$$\theta_{out}=\alpha+\frac{V'_B}{V_z(0)}\,. \tag{11}$$

The previous reasoning has been done on a single atom, entering the interaction region with a velocity $V_z(0)$ along $\mathbf{e}_z$. Consider now the whole atomic beam. Owing to both the initial divergence of the atomic beam and the dispersion of longitudinal velocities, $V_z(0)$ is not the same for all the atoms. According to equation (11), the output angle θ_{out} thus has a distribution, due to the obvious dependence on $V_z(0)$ of the second term, and also to the dependence of V'_B on $V_z(0)$:

$$V'_B=\frac{\delta}{k}+\frac{1}{k}\sqrt{\hbar k\frac{\Gamma}{2}\frac{\omega_1^2}{2}\frac{R}{M(V_z(0))^2}-\frac{\omega_1^2}{2}-\frac{\Gamma^2}{4}}\,. \tag{12}$$

Note that V'_B depends also on the point P where the atom enters the interaction region but the variation is small compared to the distance R = OP. An interesting situation happens when the first term of equation (11), α, that is independent of the longitudinal velocity, is the dominant contribution to θ_{out}. In this case, all atoms have the same final transverse velocity : the atomic beam is thus strongly collimated around the direction defined by α. This situation

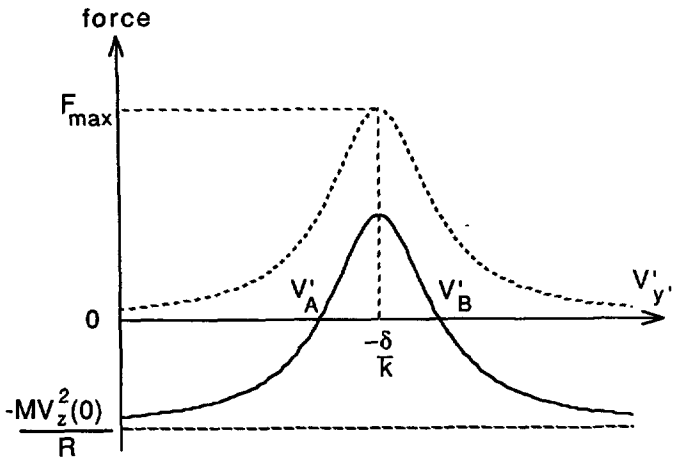

Fig. 16. — Total force determining the motion of an atom in the rotating frame $\mathcal{R}'$. This force, which is the sum of the radiation pressure force (Lorentzian contribution) and of the inertial centrifugal term (constant), is plotted as a function of the transverse velocity $V'_{y'}$ in $\mathcal{R}'$. V'_A and V'_B correspond to steady state solutions of the equation of motion : the first solution is unstable, the second one is stable.

also corresponds to a larger increase of the deflection due to the converging laser beam, compared to the case of a plane wave. As a matter of fact, the deflection in the case of a plane wave is limited by the width of the spontaneous force, i.e., it is of the order of $V'_B/V_z(0)$.

All the discussion above is valid only if the locking point V'_B exists. It is clear in figure 16 (or Eq. (9)) that this imposes :

$$R > R_{min} \tag{13a}$$

with

$$R_{min} = M\frac{(V_z(0))^2}{F_{max}} = M\frac{(V_z(0))^2}{\hbar k\dfrac{\Gamma}{2}}\frac{\omega_1^2/2 + \Gamma^2/4}{\omega_1^2/2} \tag{13b}$$

This condition expresses the fact that the centrifugal force must not exceed the maximum value of the radiation pressure.

5.3 EXPERIMENTAL RESULTS. — In order to illustrate the previous discussion, we present a deflection experiment performed on the helium beam in the configuration shown in figure 14. The ground state helium atoms, at room temperature, are bombarded with 23 eV electrons. The average longitudinal velocity is about 1 500 m/s. The LNA laser is locked on the resonance ($\delta = 0$) of the $2\,^3S_1 \leftrightarrow 2\,^3P_2$ transition. Its output beam is expanded with a telescope and has a waist diameter of about 30 mm in the interaction region and an intensity corresponding to a Rabi frequency $\omega_1 = 6.3\,\Gamma$. The convergence of the laser beam is adjusted by changing the distance between the two lenses of the telescope. The deflection of the atoms is measured by scanning the detector placed 1.6 m downstream of the interaction region.

Figure 17 shows the evolution of the transverse atomic profiles as the convergence of the laser beam is increased (radius R decreased). The angle of deflection increases as we reduce R from infinity (plane wave, curve b) down to 6 meters. The mean deflection angle (corresponding to the top of the deflected peak) is two times larger (8 mrd) for a radius of

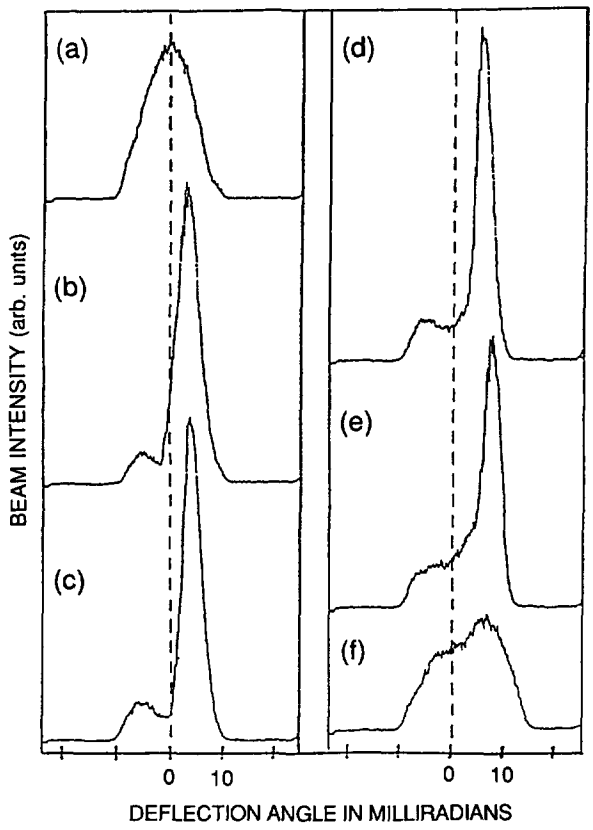

Fig. 17. — Transverse profiles of the metastable helium atomic beam interacting at right angles with a converging laser travelling wave (radius of curvature R), as a function of the deflection angle. (a) laser off ; (b) plane laser wave $R = \infty$ ($I = 80\, I_{sat}$, $\delta = 0$) ; (c) $R = 20$ m ; (d) $R = 10$ m ; (e) $R = 6$ m ; (f) $R = 4$ m. Note that here the deflection angle is measured with respect to the mean direction of the initial atomic beam.

6 meters than for a plane wave. We also observe that, for a radius of curvature between 6 and 4 m (see curves e and f), the deflection method ceases to work, which is in good agreement with the minimum radius $R_{min} = 5$ m calculated with formula (13b). Besides the deflection, the converging laser beam clearly collimates the atomic beam around its mean direction (see the narrowing of the atomic beam profile for instance in Fig. (d)). According to the discussion above, this collimation is limited by the distribution of longitudinal velocities in the atomic beam (see Eq. (12)) : the contribution $V'_B/V_z(0)$ to the deflection angle is not small compared to α (see Eq. (11)), because of the short interaction time, and it varies by $\pm$ 1.5 mrd when the longitudinal velocity $V_z(0)$ varies by $\pm$ 10 %. Note also that it is difficult to make a full quantitative comparison with the discussion above because our interaction time (about 20 μs) is of the order of the time constant of the velocity damping towards V'_B (30 μs at best in our situation, with a radius of curvature $R = 2\, R_{min}$). In our experiment, the best collimation is obtained in the curve (d) of figure 17, that corresponds to the strongest damping ($R = 10$ m $= 2\, R_{min}$).

6. Conclusion.

In this paper, we have described a LNA laser suitable for the manipulation of metastable helium by radiation pressure forces. A specific feature of this laser is the frequency stabilization on the $2\ ^3S \leftrightarrow 2\ ^3P$ transition atomic line in a discharge cell, realized with a single feedback loop. This has been made possible by using a F.M. saturated absorption spectroscopy technique. With a relatively simple implementation, this scheme yields a laser linewidth of 130 kHz, with a long term reproducibility better than 400 kHz. These performances are widely sufficient for radiation pressure experiments with an atomic linewidth of 1.6 MHz. If necessary, the performances could be much improved according to the suggestions made in section 3.3.

We have presented two examples of the usefulness of laser manipulation of metastable helium. The first one allows us to increase the atomic density in the beam axis by compression of the transverse velocity distribution. The second one is a transverse deflection of the atomic beam with a converging laser beam, and it also yields a compression of the transverse velocity distribution. Such techniques, which require only a few milliwatts of laser light, are currently used in our laboratory. They are specially interesting in the case of metastable helium, which is produced with a low efficiency in a beam containing mostly helium in the ground state. These techniques provide separation and density increase of the $2\ ^3S$ metastable atoms. We have also indicated how a related method (« anticooling ») allows us to check the beam purity in triplet metastable atoms.

In section 5, we have given a detailed analysis of the mechanism underlying the deflection with a curved laser wavefront. In a proper rotating frame of reference, the transverse motion of the atoms is found to be described by a total force (Fig. 16) exhibiting two equilibrium points, one stable and one unstable. Here we have considered only the steady state motion due to this force. On the other hand, the transient regime presents some more complex features, that may lead to a bistable behavior [35]. For instance, with the addition of a second transverse spherical laser wave, we would realize a genuine bistable system, in the spirit of [36]. This system would offer a wide choice of possible control parameters (laser frequencies and intensities, radius of curvature and focusing points of the wavefronts, ...). This scheme might be of interest for switching an atomic beam between several positions.

We express our warm thanks to M. Leduc, who pioneered the work on LNA lasers, and who shared with us all her knowledge as well as many specific optical parts. We thank MM. Wyon and Aubert, from LETI, who provided us with the LNA crystals. We acknowledge a very useful help from H. Haberland and M. Karrais for the atomic beam apparatus, and many fruitful discussions with C. Cohen-Tannoudji and J. Dalibard.

This work has been partially supported by the stimulation program of European Economic Community, and by Direction des Etudes et Recherches Techniques (grant 89214). One of us (C.G.) acknowledges a grant from the Deutsche Forschungsgemeinschaft. The participation of L. H. has been supported by a NATO grant.

References

[1] The Mechanical Effects of Light, *J. Opt. Soc. Am.* **B 2** (1985) special issue.

[2] Laser Cooling and Trapping of Atoms, *J. Opt. Soc. Am.* **B 6** (1989) special issue.

[3] SHIMIZU F., SHIMIZU K. and TAKUMA H., *Phys. Rev.* **A 39** (1989) 2758.

[4] SALOMON C., DALIBARD J., PHILLIPS W. D., CLAIRON A. and GUELLATI S., *Europhys. Lett.* **12** (1990) 683.

[5] ASPECT A., VANSTEENKISTE N., KAISER R., HABERLAND H. and KARRAIS M., *Chem. Phys.* **145** (1990) 307.
[6] NELLESSEN J., WERNER J. and ERTMER W., *Opt. Commun.* **78** (1990) 300.
[7] RIIS E., WEISS D. S., MOLER K. A. and CHU S., *Phys. Rev. Lett.* **64** (1990) 1658.
[8] STEANE A. M. and FOOT C. J., *Europhys. Lett.* **14** (1991) 231.
[9] ZHAO P., LAWALL J. R., KAM A. W., LINDSAY M. D., PIPKIN F. M. and LICHTEN W., *Phys. Rev. Lett.* **63** (1989) 1593.
[10] ASPECT A., ARIMONDO E., KAISER R., VANSTEENKISTE N. and COHEN-TANNOUDJI C., *Phys. Rev. Lett.* **61** (1988) 826.
[11] BAUDON J., PERALES F., MINIATURA Ch., ROBERT J., VASSILEV G., REINHARDT J. and HABERLAND H., *Chem. Phys.* **145** (1990) 153.
[12] SESSELMANN W., WORATSCHEK B., KUPPERS J., ERTL G. and HABERLAND H., *Phys. Rev. B* **35** (1987) 1547.
[13] SCHEARER L. D., LEDUC M., VIVIEN D., LEJUS A. M. and THERY J., *IEEE J. Quant. Elect.* **QE22** (1986) 713 and references therein ;
AMINOFF C. G., LARAT C., LEDUC M. and LALOE F., *Rev. Phys. Appl.* **24** (1989) 827.
[14] HAMEL J., CASSIMI A., ABU-SAFIA H., LEDUC M. and SCHEARER L. D., *Opt. Commun.* **63** (1987) 114.
[15] CHUANG T. and METCALF H., *Appl. Opt.* **30** (1991) 2495.
[16] LETI : C.E.N.G., BP 85X, 38041 Grenoble. We acknowledge in particular Ch. Wyon and J. J. Aubert for their help.
[17] See for instance : KASTLER A., BRUHAT G., Optique, 5e édition, Masson (Paris, 1959), p. 470 ; YARIV A., YEH P., Optical waves in crystals (Wiley, 1984), p. 152.
[18] BLOOM A. L., *J. Opt. Soc. Am.* **64** (1974) 447.
[19] See for example : SIEGMAN A. E., Lasers, p. 954-957 (Univ. Sc. Books, Mill Valley, CA, 1986), p. 954-957.
[20] DREVER R. W. P., HALL J. L., KOWALSKI V., HOUGH J., FORD G. M., MUNLEY A. J. and WARD H., *Appl. Phys.* **B 31** (1983) 97.
[21] BJORKLUND G. C., *Opt. Lett.* **5** (1980) 15 ;
BJORKLUND G. C., LEVENSON M. D., LENTH W. and ORTIZ C., *Appl. Phys.* **B 32** (1983) 145.
[22] BLOCH D., RAJ R. K. and DUCLOY M., *Opt. Commun.* **37** (1981) 183.
[23] Although in this configuration the $LiTaO_3$ crystal induces only a phase modulation, the interference between the reflections on the two faces of the crystal transforms the modulation of the index of refraction into an amplitude modulation. This effect is important with uncoated $LiTaO_3$ because of its high index of refraction (around 2.13), and it leads to an offset on the detected signal at Ω. It can be reduced by tilting the crystal or with a good AR coating.
[24] BARGER R. L., SOREM M. S. and HALL J. L., *Appl. Phys. Lett.* **22** (1973) 573.
[25] It is well known that intensity fluctuations of the pump induce frequency fluctuations on the laser. These fluctuations may then be correlated for our two LNA lasers pumped with the same argon laser, but this effect is not important at the 100 kHz level achieved here.
[26] BARGER R. L., WEST J. B. and ENGLISH T. C., *Appl. Phys. Lett.* **27** (1975) 31 ;
HALL J. L. and HÄNSCH T. W., *Opt. Lett.* **9** (1984) 502.
[27] BRUTSCHY B. and HABERLAND H., *J. Phys. E* **10** (1977) 90.
[28] FAHEY D. W., PARKS W. F. and SCHEARER L. D., *J. Phys. E* **13** (1980) 381 ;
RUF M.-W., YENCHA A. J. and HOTOP H., *Z. Phys. D* **5** (1987) 9 ;
VERHEIJEN M. J., BEIJERINCK H. C. W., v. MOLL L. H. A. M., DRIESSEN J. and VERSTER N. F., *J. Phys. E* **17** (1984) 904.
[29] RADZIG A. A. and SMIRNOV B. M., « Reference Data on Atoms, Molecules and Ions », p. 251, Ed. J. P. Toennier (Springer-Verlag, 1985).
[30] In the case of a laser intensity not small compared to I_{sat}, the total average force is not the sum of the two forces from the two travelling waves, since coherent effects between the two waves must be taken into account (see Minogin V. G. and Serimaa O. T., *Opt. Commun.* **30** (1979) 373). However, for a Rabi frequency small enough ($\omega_1 \leq 10\,\Gamma$) and for a detuning on the order of or larger than the Rabi frequency ($|\delta| \geq \omega_1$), the variation of the force as a function

of the velocity is qualitatively the same as the one in figure 12 (the maximum value being close to $\hbar k(\Gamma/2)/(1 + \Gamma^2/2\,\omega_1^2)$).

[31] HÄNSCH T. W. and SCHAWLOW A., *Opt. Commun.* **13** (1975) 68 ;
WINELAND D. and DEHMELT H., *B.A.P.S.* **20** (1975) 637.

[32] FRISCH R., *Z. Phys.* **86** (1933) 42 ;
JACQUINOT P., LIBERMAN S., PICQUE J. L. and PINARD J., *Opt. Commun.* **8** (1963) 163 ;
SCHIEDER R., WALTHER H. and WOSTE L., *Opt. Commun.* **337** (1972) 337.

[33] In our situation the radius of curvature of the laser wave will be of the order of a few meters, and can be considered as a constant over the whole interaction region (which is a few mm wide). All the atoms from the beam will therefore see the same laser intensity. This situation is very different from the experiment described in NELLESEN J., MULLER J. H., SENGSTOCK K. and ERTMER W., *J. Opt. Soc. Am.* **B 6** (1989) 2149.

[34] In fact, as usual in laser cooling, the steady-state situation results from the equilibrium between the average friction mechanism around V_B' and diffusion processes due to the random character of absorption and spontaneous emission of photons. The final velocity spread around V_B' could easily be calculated using the method given in : SALOMON C. and DALIBARD J., *C.R. Acad. Sci. Paris* **306** (1988) 1319.

[35] BONIFACIO R. and LUGIATO L. A., *Opt. Commun.* **19** (1976) 172 ;
LUGIATO L. A., in *Progr. Opt.* Vol. **21,** edited by E. Wolf (North-Holland, Amsterdam, 1984).

[36] ASPECT A., BONIFACIO R., CASAGRANDE F. and LUGIATO L. A., *Eur. Phys. Lett.* 7(6) (1988) 499.